Spectral reflectance properties of sand layers covering an underlying target– experimental measurements and mathematical modelling

Gorm Krogh Selj,[a, *] Alexander Mikkelsen[a]
[a]Norwegian Defence Research Establishment, Instituttveien 20, 2007 Kjeller, Norway

ABSTRACT

Adapting to natural backgrounds is important, yet very difficult, to achieve effective camouflage. One interesting aspect is the optical depth of biomaterials as a function of both geographical region, in which the biomaterials exist, and wavelength. The effective optical thickness of sand, for instance, will vary from scene to scene, and the amount of light that is reflected and transmitted is lower in the visible wavelength region than in the near-infrared region. Such variations in optical properties should be accounted for to ensure that synthetic camouflage material has high adaption to natural backgrounds over a large set of natural scenes as well as over a large range of wavelengths. The aim with this study has been to study optical reflectance properties of thin sand layers as a function of their thickness, given in weight per area. Sand is a biomaterial abundant in many parts of the world and relevant for many camouflage purposes. In specific, we have studied spectral reflectance (350–-2500 nm) of 1–6 layers of sand covering a generic target object with known spectral signature. We also present mathematical models aiming to be able to estimate the reflectance of the sand layer samples, for a given layer thickness. The models are easy to use and we show that the models are able to reproduce the spectral reflectance properties of the sand samples. The model also allows for an estimation of the optical extinction coefficient as a function of wavelength and for a given sand type. This opens for a further estimation of transmittance and absorptance of the sand layers based on the experimental reflectance data, and we explore this in the paper. We also explore how the model is able to capture optical properties of sand and compare with corresponding optical properties of other natural materials, often found in thin layers, such as leaves and snow. We think our results will be a valuable contribution to developing multi-layered camouflage material that accounts for the variation of optical depth.

Keywords: sand, spectral imaging, reflectance, transmittance, camouflage materials, mathematical models.

***Gorm Krogh Selj, E-mail: gorm-krogh.selj@ffi.no

1 INTRODUCTION

Sand reflectance is interesting from a camouflage point of view as various types of sand are found in many parts of the world. Sand reflectance of incident light differs from light reflected by other natural materials or constituents, such as vegetation, soil, snow and ice, as well as from many synthetic products, by its unique spectral signature in the wavelength region 350 – 2500 nm, containing light in the UV, visible range, near-infrared range and SWIR. In addition, sand materials are porous, easily moveable (also by winds), meaning that they are interesting candidates as natural camouflage materials in many situations as well as the assumption that a thin sand layer will transmit some of the incident light, makes it interesting to characterize its optical properties further.

In the years to come, electro-optical sensors are thought to become cheaper, more capable, globally distributed and smaller and lighter. In addition, data analysis methodologies become more accessible, tailored and sophisticated, and remote sensing applications, including drones, are expected to become more important. In light of this expected development, we expect that successful concealment of an object will become increasingly challenging and will require camouflage materials (or strategies) that are well adapted to the optical characteristics of the backgrounds considered relevant.

The interaction of incident solar radiation with sand materials (of various thickness and granularity) will be interesting to study in order to develop camouflage strategies in sand-dominated areas [1-8]. In addition, precise interpretations of signatures captured by remote sensors will be important in land mapping based remote sensing application as is likely to

Target and Background Signatures IX, edited by Karin Stein, Ric Schleijpen,
Proc. of SPIE Vol. 12736, 1273609 · © 2023 SPIE
0277-786X · doi: 10.1117/12.2680343

rely on a thorough understanding of land optical materials, such as sand. Sand is a granular material with complex microstructure and varying density. Since sand materials are normally not optically opaque, but semi-transparent, some incident light may penetrate a (thin) sand layer as a function of wavelength and layer thickness. The wavelength distribution and amount of incoming light transmitted through a sand layer will affect the signature that any optical sensor will capture. It is also of interest to compare the light transparencies of various layer-like materials found in nature [9-14], to gain more knowledge on how much light different materials will reflect, transmit and absorb as a function of wavelength and thickness. It has already been reported on optical similarities between soil-materials and snow when they have been studied on length scales much larger than the wavelength [13]. This study aims to build further knowledge on optical characteristics of one of the natural materials, sand, that is naturally found in layers.

In this paper, we have measured spectral reflectance of a given sand material when the sand material has been used as layer material on top of an underlying reference textile with well-defined signature. The sand was placed in layers of varying thickness on top of the textile to study how much of the initial textile reflectance signature is left in the reflectance spectra as the sand layer was increased in steps. We have also applied a mathematical model, the extinction model [9, 15], to the reflectance data. We investigated the applicability of the mathematical model, used in a predicative sense, to see if it is able to model sand optical parameters, such as extinction coefficients and reflectivity, correctly. We also investigated the potential of the model giving reliable estimations and answers to problems that are considered difficult to solve by direct experiments, such as sand layer transmittance and absorptance. Extinction coefficients of sand were calculated for selected wavelengths (500nm, 800 nm, 1200 nm, and 1800 nm) by using a mathematical model for thin and optically semi-transparent materials [11, 15] win combination with our experimental data. The application of the model to experimental reflectance data allows for wavelength-dependent estimations of sand inherent reflectivity (inherent property of sand, no influence from any background object) and transmittance characterizations.

We expect the results found in this preliminary study to be of value in several applications involving light penetration in thin materials [16]. One candidate is further improvements in advanced camouflage products [17-20] or in camouflage assessment techniques[17, 18, 21-34]. Other potential applications may be within solar energy harvesting [35-43], in which a thin layer of sand material on the solar module surfaces may hamper the energy harvesting effectivity substantially, in fields related to planetary sciences[41, 44, 45], as well as for remote sensing applications [13, 27, 46-50] of land areas or objects where the mapping accuracy, including sand and soil type predictions [51-53], may be affected by thin sand (or soil) layers covering vegetation or other interesting infrastructure.

2 EXPERIMENTAL SETUP AND METHOD

2.1 Spectral measurements

The reflectance spectra of the sand layer samples were measured outdoors in natural light (sunny, clear sky) by a field spectrophotometer (Spectra Vista SVC 1024 UV/VIS/NIR/SWIR) between 350 and 2500 nm. The spectrometer was connected to a laptop to control the measurements via the program SVC HR1024 (v. 1.7). The distance between the samples and the spectrophotometer was around 1 meter, yielding a measurement area of about 5x5 cm^2. The spectrophotometer was slightly tilted to reduce the degree of specular reflectance from the samples. A Lambertian white reference plate (Spectralon calibrated diffuse reflectance standard, PerkinElmer) was used between each measurement series to calibrate the instrument. We measured the samples at least five times, with a fixed measurement time of 1 second. The spectral results presented in the paper (section 4.1) are an average of five or more spectral measurements for each sample. All reflectance measurements were performed on hard ground (sand-covered open field) in Canjuers, France, during summer. An overview of the experimental setup is presented in Figure 1.

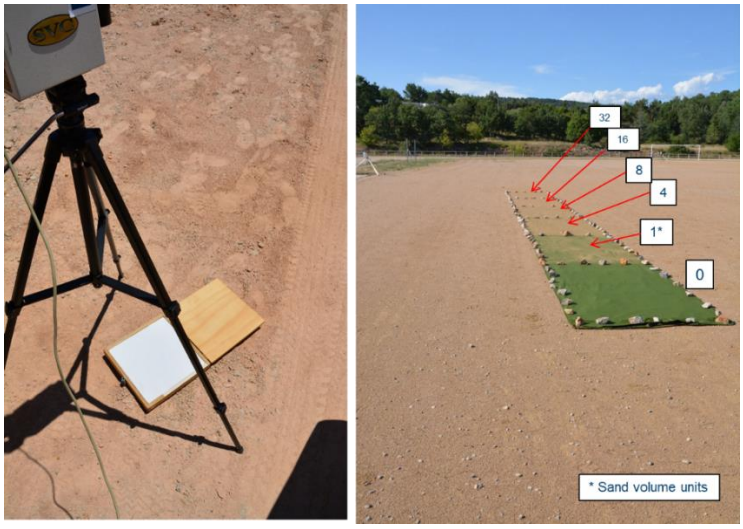

Figure 1. Experimental setup. (a) field spectrophotometer (Spectra Vista SVC 1024 UV/VIS/NIR/SWIR) and (b) sand layers on top of a green reference target (are approximately 3.3 m^2). The sand layer samples were measured individually outdoors under stable illumination conditions (clear sky). A white reference plate (Spectralon calibrated diffuse reflectance standard, PerkinElmer) was used before measuring the reflectance of each sand layer.

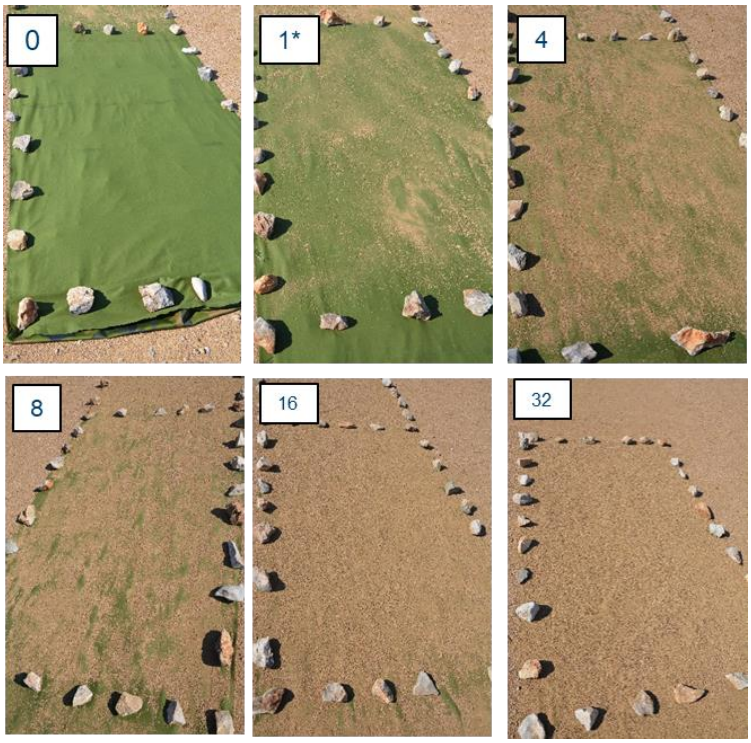

Figure 2. Sand layers on top of a green reference textile for spectral reflectance measurements. The top left image shows the textile with no sand placed onto it ("textile reference"). The sand volume units used are shown in the top left corner of the remaining samples and the sand was evenly distributed over the equally sized sample areas, respectively.

We measured the reflectance of each of the different sand layer thicknesses individually (with a green textile underneath), and a measurement series of pure sand (no textile underneath). The samples (sand layers) measured are shown in Figure 2. The samples, altogether 7, consisted of the reference textile covered with no sand, 1, 4, 8, 16, and 32

volume units of sand, as well as the pure sand sample (no textile underneath). A volume unit consisted of 1 liters of sand, and the sand volumes were evenly distributed over the equally sized reference textile areas, respectively. All sand samples used in the textile coverages were obtained from the ground next to the reference textile, and the sand is assumed to be of the same type in the measurements. The mass density of the sand was not measured, but we assumed the sand density to be of 1.631 g/cm^3 (US customary measurement system) in our transmittance modelling calculations. However, the modelling is meaningful regarding sand layer transmittance estimations as long as all the layers we used in our experiments were of the same type and by controlling the sand volume for each layer. The estimated (optical transmittance) material parameter, the extinction coefficient *k*, will however be influenced by the estimated mass per density value of each sand layer we used in this experiment. Therefore, we have estimated sand mass (of each sand layer) as well as measured each sand sample area (see Fig. 2) as accurately as we were able to. The spectrophotometer saved the spectral data as .sig files that we analyzed and plotted in Origin Pro 2021 (v. 9.8.0.200). All the spectral measurement results presented in this paper are mean values from several measurements.

3 THEORETICAL MODEL OF LIGHT REFLECTANCE OF SAND LAYERS

The spectral reflectance data in this paper is fitted with a mathematical model, here named the extinction model. In this section, we will introduce the model and show how it can estimate the spectral properties of samples based on multilayered spectral measurements.

3.1 The extinction model

The extinction model has been used in recent studies to model the light reflectance and transmittance from thin and layered samles as a function of layer thickness (given by the layer mass/area) [9-12]. Wilhelm [15] derived the extinction model to describe quantitatively the reflectance, transmittance, and absorptance in terms of specific reflection and absorption characteristics of fibers. The model is based on the Stokes equations[54] for transmittance t_n and reflectance r_n of n plates:

$$t_n = \frac{c-c^{-1}}{cd^n-c^{-1}d^{-n}}, \tag{1}$$

$$r_n = \frac{d-d^{-n}}{cd^n-c^{-1}d^{-n}}, \tag{2}$$

where *c* and *d* are constants that only depend on the reflectance and transmittance of the single plates. The equations above were fitted to textile materials of different thicknesses expressed as weight per area by defining $c = 1/\alpha$ and $d = e^k$. Here the constant α is the reflectivity of the material when the thickness goes towards the extreme limit, k the extinction coefficient, while the constant e^{-kw} is the remaining energy fraction after absorption in a unit weight per area w of the material. Substituting n with w, which is the weight per unit area, and using the new definitions yield[15]:

$$t_w = \frac{(1-\alpha^2)e^{-kw}}{1-\alpha^2e^{-2kw}}, \tag{3}$$

$$r_w = \frac{\alpha(1-e^{-2kw})}{1-\alpha^2e^{-2kw}}. \tag{4}$$

The corresponding absorptance is then given by the following relationship: a_w = 1 - r_w - t_w.

For semi-transparent samples (such as snow, vegetation, and thin artificial material) we have to account for the optical characteristics of both the i) sample and the ii) underlying background[9, 14]. The spectral characteristics of the background must therefore be included for correct modeling. If the reflectance of the background is given by β, expressions for the reflected, transmitted, and absorbed light of the system (sample and background)are given by[15]:

$$\left(\frac{I_r}{I_0}\right)_{\text{syst.}} = r_w + t_w^2\beta + t_w^2r_w\beta^2 + t_w^2r_w^2\beta^3 + \cdots = r_w + \frac{t_w^2\beta}{1-r_w\beta}, \tag{5}$$

$$\left(\frac{I_t}{I_0}\right)_{\text{syst.}} = t_w(1-\beta) + t_wr_w\beta(1-\beta) + t_wr_w^2\beta^2(1-\beta) + t_wr_w^3\beta^3(1-\beta) \ldots = \frac{t_w(1-\beta)}{1-r_w\beta}, \tag{6}$$

$$\left(\frac{I_a}{I_0}\right)_{\text{syst.}} = 1 - \left(\frac{I_r}{I_0}\right)_{\text{syst.}} - \left(\frac{I_t}{I_0}\right)_{\text{syst.}} = \frac{a_w(1+\beta)(t_w-r_w)}{1-r_w\beta}. \tag{7}$$

4 RESULTS – REFLECTANCE

4.1 Reflectance of multiple layered sand samples

Figure 3 shows the measured reflectance of the individual sand layers given by the sand volume used to cover the underlying green reference target. The green curve shows the reflectance of the uncovered reference textile, and the red curve shows the reflectance of pure sand (no textile underneath), whereas the remaining curves in Fig. 3 show the reflectance for the different sand layer thicknesses (with the reference textile beneath). It was not possible to measure the sand layer thickness during the experiment, but the layers are instead characterized by the amount (i.e. volume) of sand used to create each layer. We see from Figure 3 that the reflectance spectra of the various sand layer thicknesses (as well as the bare reference textile) were all different over the wavelength range, meaning that varying the sand thickness, when covering some underlying target, seems to alter (i.e. reduce) the spectral reflectance signature that is measured.

Furthermore, we note that the reflectance characteristics of the five sand layers (1 L to 32 L) were in general obtaining reflectance values between those of the bare reference textile (green curve) and pure sand (red curve). This observation agrees with what we would expect as all the reflectance curves of the sand layers covering the reference textile should be some mix of reflectance signatures of the reference textile and sand. In Figure 3 we see that as the sand layers got thicker, the corresponding reflectance curves got more similar relative to the reflectance curve of pure sand. Correspondingly, the impact of the reference textile signature on the measured reflectance (of the reference textile covered with sand) was rapidly reduced as the sand layers got thicker. We also note that there was one wavelength, at about 860 nm, where all the reflectance curves obtained the same reflectance values, meaning that all the sand layers, the bare textile and the pure sand sample were undistinguishable by their reflectance value at that particular wavelength. In addition, at the wavelength region between ca. 2050 nm and 2150 nm the reflectance values of the five sand layers did not obtain values between that of the bare textile reflectance (green curve) and that of the pure sand (red curve), but seemed to be slightly higher in reflectance than both. This was not as expected, and there was no obvious explanation to this other than potentially measurement errors (in that particular wavelength range).

From Figure 3 we see that the reflectance of the sand layer samples had the largest variations for wavelength regions around 650 nm and for the wavelength range of approximately 900 nm to 1300 nm. In particular, the variation in reflectance was significant in these two region when altering the sand layer thickness as in our study. We also find, when inspecting the curves in Figure 3, that the reflectance altered noticeably between 0 L (no sand, green curve), 1 L (purple curve), 4 L (orange curve), 8 L (brown curve), but to a less degree (albeit observable) between 8 L (brown curve), 16 L (pink curve), 32 L (grey curve) and pure sand (red curve). We could not measure the corresponding sand layer thicknesses. Still, they can be estimated (assuming the sand volume was evenly distributed throughout the textile area) to be 0.3 mm (1 L, thinnest layer), 1.2 mm (4 L, second layer), 2.4 mm (8 L, third layer), 4.8 mm (16 L, fourth layer), and 9.7 mm (32 L, fifth layer). The observed variations in measured reflectance with altered sand layer thickness is interesting as we would like to know more about what sand layer thickness that cover a buried target to a sufficient degree, and what is the expected layer thickness (of some layer constituent) that alters the measured signature from being dominated by the target signature to being dominated by the layer constituent signature.

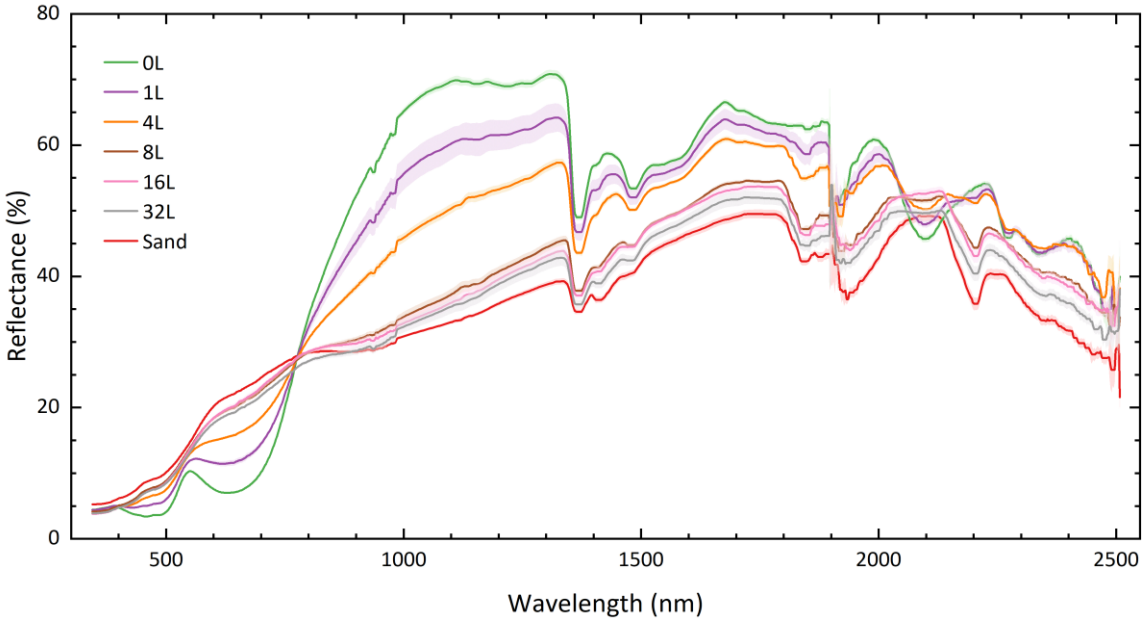

Figure 3. Spectral reflectance measurements of sand layers covering a green reference target, given by the amount of sand (in liters). Reflectance of no sand layer is given by the green line, 1 liter sand to cover the target (purple line), 4 liters (orange line), 8 (brown line), 16 liters (pink line), 32 liters (grey line), and pure sand with no target underneath (red line) between 345 nm and 2500 nm. The shaded bands behind the lines represent the standard error of the reflectance mean (errors smaller than the lines might not be visible in the plot).

From the results in Figure 3, we may speculate if the sand layer thickness that shifts the signature from target-like to sand material-like could be around the thicknesses from 4 to 8 layers. Comparing the reflectance measurements (Fig. 3) with images in the visual range of the corresponding sand layers (Fig. 2), there seems to be a clear visual impression between the image of the 4 L thickness and the 8 L thickness regarding how much of the underlying target we can see (in the visual wavelength range). However, it is not possible to draw any conclusion based on the visual impressions given in Figure 2. Interestingly, we also see from Figure 3 that even for the thickest sand layer, 32 L (grey curve), the corresponding reflectance curve did not seem to overlap with the reflectance curve of pure sand (red curve), indicating that there is some amount of light that penetrated the sand layer, reaching the underlying reference target and then being reflected back from that target through the sand layer and back to the external spectrophotometer. Particularly at wavelengths around 950 nm to 1300 nm the transition of incoming light through a relatively thick sand layer seemed most prominent.

In figure 3, we see that the reflectance data of the thinnest of the sand layers, 1 L (purple curve) had the highest uncertainty (SE) in the sand layer measurements. This is because it was difficult to homogeneously distribute the smallest amount of sand (1 L) onto the textile area. The images of the sand layers in Figure 2 also clearly shows how the large degree on non-homogeneity of the sand distribution for the sand layer, and that the homogeneity of the sand layers, in general seemed to increase when the amount of sand was increased.

4.2 Fitting the extinction model to the reflectance data

Having converted the number of layers to mass per area (see Table 1 for numeric values), we fitted the extinction model (Eq. 5) to the measured reflectance data of the individual sand layers, as shown in Figure 4. We selected eight test wavelengths over a range from 550 nm to 2200 nm to carry out a preliminary test of the model fit to the data. We fitted the data by adjusting two fitting parameters: the reflectivity (α) and extinction coefficient (k), following the approach used in other studies [10-12]. The 8 wavelengths were chosen based on the reflectance curves of the sand layers (Fig. 3) and to be spread out to cover VIS, near infrared (NIR), and shortwave infrared (SWIR) wavelength ranges. The fitting parameters and the selected wavelengths are shown in Table 1. In Figure 4, we show the experimental reflectance data of the five sand layers (1 L of sand corresponding to a layer thickness of 0.05 g/cm^2, and up to 32 L corresponding to 1.6 g/cm^2) plotted against the estimated mass per area for the wavelengths 550 nm, 800 nm, 1200 nm, and 1800 nm. In Figure 3 we also plot the corresponding model fit (blue curves) when the extinction model was applied to the experimental data.

From Figure 4 we see that at 550 nm (Fig. 4 (a)) the reflectance values were low (ca. 6 %) initially (i.e. for the thinnest sand layer, approximately 0.05 g/cm^2) and increasing for the second and third sand layer thickness (8-9 % reflectance at 0.2 and 0.40 g/cm^2, respectively), and remained relatively constant when the sand layer was further increased up to the two thickest layers at 0.79 and 1.58 g/cm^2. This corresponds with what we see from the reflectance values in Figure 3 at 550 nm where the reflectance changed during the first thinnest layers (0 L to 4 L in Fig. 3) and then converged towards a fixed value for the thicker sand layers. Furthermore, we see that the model fitted the experimental data well (blue curve) at 550 nm.

The remaining three wavelengths shown in Figure 4 ((b) 800 nm, (c) 1200 nm, and (d) 1800 nm) all show the same reasonably well model fit to the experimental data. At these three wavelengths the reflectance decreased with increasing sand layer thicknesses, that is the reflectance values in Figure 4 (b) - 4(d) decreased as the weight per area was increased. As for the model fit at 550 nm, the model fit at 800 nm, 1200 nm, and 1800 nm converged towards a fixed reflectance value for increasing weight per area of sand.

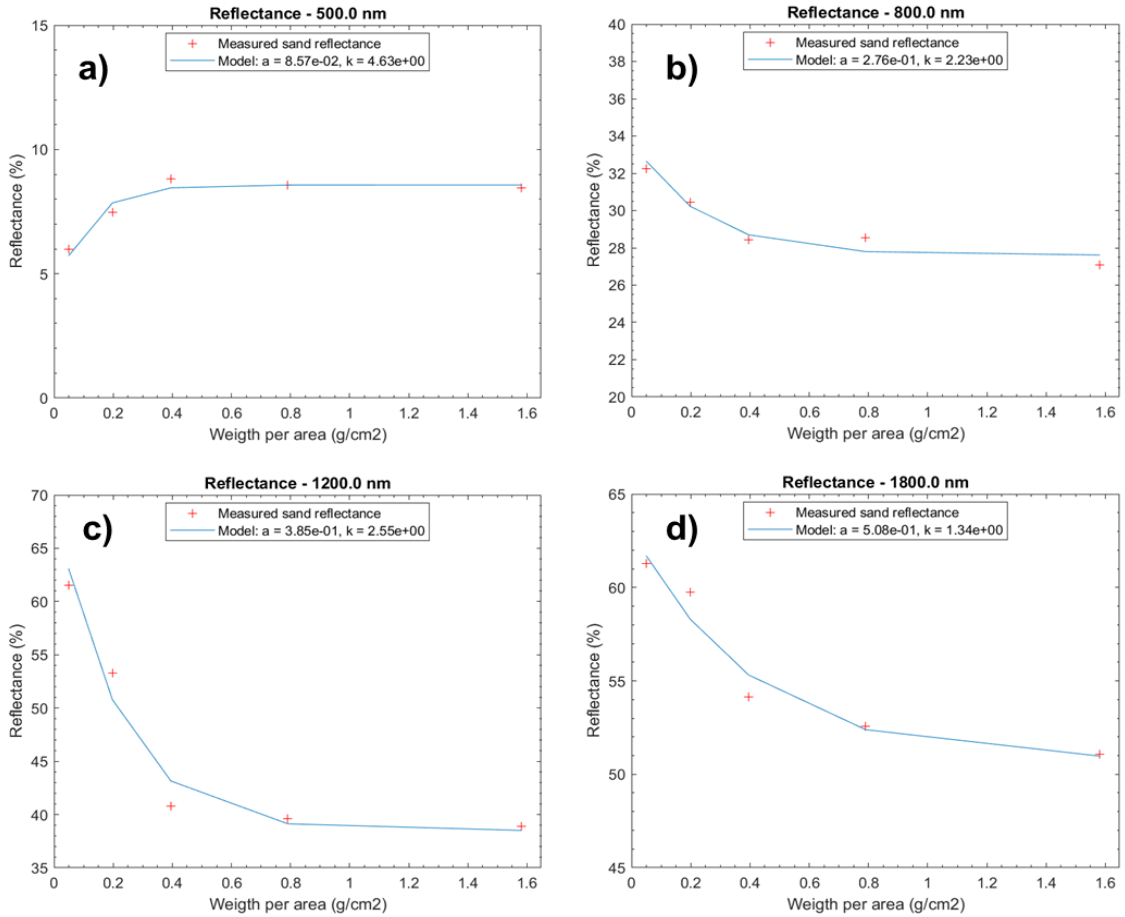

Figure 4. Reflectance plotted against mass per area for the sand layers at (a) 500 nm, (b) 800 nm, (c) 1200 nm, and (d) 1800 nm. The blue solid line represents the estimated reflectance from fitting the data to the extinction model.

The extinction model (blue curves in Fig. 4) fitted well with our experimental reflectance data for all the selected wavelengths. The reflectivity parameter used for fitting data to the model is similar to the reflectance of the samples at the highest mass per area, i.e. for the thickest sand layers. The fitting parameter is similar to the asymptotic reflectance value when the sand layer thickness approaches infinity. At the same time, the *extinction coefficient* describes how quickly the sample reflectance converges towards the reflectivity value as a function of increased thickness. High extinction coefficient values mean that the sample absorbs much of the incoming light and that a thinner layer is sufficient to effectively reduce the reflectance contribution from the underlying target, on the measured reflectance. This means that a sample with high extinction coefficient would obtain a flat reflectance-versus-thickness curve. This is also why we see that the extinction

coefficient, *k*, from the fitting procedure (Table 1) is high at wavelengths where the samples had smaller variations in reflectance with thickness, and low at wavelengths where the reflectance changed more markedly with thickness of the sand layer sample.

From Figure 4 this observation seems to correspond with the visual impression of the 4 curve fits (550 nm, 800 nm, 1200 nm, and 1800 nm). In Figure 4 we see that the 550 nm fit curve (blue curve, Fig. 4 (a)), which obtained the highest/lowest value of the extinction parameter, converged already at about 0.4 g/cm^2. In contrast, the 1800 nm fit curve (blue curve, Fig 4 (d)) did not converge entirely even at the highest mass per area value at 1.58 g/cm^2. This means that at 1800 nm some light still reaches the underlying textile sample through the thickest sand layer (1.58 g/cm^2) used in this study, and that ideally reflectance measurements on even thicker sand layers should have been conducted. This means that some incident light at 1800 nm will penetrate a sand layer of about 3 cm (with the sand mass density as used in our calculations) and with a sand type similar to what we used to cover the reference textile. In summary, this shows that the extinction coefficient seems to be a valuable parameter in estimating how thick a sand layer needs to be at different wavelengths in order to the masked object to achieve the same signature as the sand itself.

Table 1. Extinction model fitting parameters. Reflectivity (α) and extinction coefficients (*k*, unit: cm^2/g) from fitting the reflectance of sand layers with the extinction model for various wavelengths (λ) between 500 and 2200 nm. The boundaries of the fitting parameters were set to [0.01, 0.99] for the reflectivity and [0.01, 10] for the extinction coefficient.

λ (nm)	**α**	***k***
500	0.09	4.6
650	0.2	3.5
800	0.28	2.2
1000	0.32	2.9
1200	0.39	2.6
1500	0.44	1.5
1800	0.51	1.3
2200	0.40	1.0

Figure 5 shows the spectral reflectance measurements (solid lines) and the estimated values (dotted lines) based on fitting the experimental reflectance data to the extinction model. We see that the experimental data (0.05 g/cm^2, red line; 0.2 g/cm^2, blue line; 0.4 g/cm^2, green line; 0.79 g/cm^2, turquoise line; 1.58 g/cm^2, purple line) captured in the wavelength region 345 – 2500 nm fitted well with the corresponding reflectance estimations based on the model (Fig. 5, dotted lines). For the three thinnest sand layers (0.05 g/cm^2, red line; 0.2 g/cm^2, blue line; 0.4 g/cm^2, green line; 0.79 g/cm^2) we see from the reflectance curves in Figure 5 that there were minor, but distinguishable, differences between the experimental data (Fig. 5, solid lines) and model fit (Fig. 5, dotted lines). For the remaining two, and thicker, sand layer thicknesses, we see that the overlap between the experimental data and the model was even better.

The results in Figure 5 show how well the model fitted the reflectance data for various sand layer thicknesses and for different wavelengths throughout the wavelength region between 345 nm and 2500 nm, covering the optical regions of UV, visual light, NIR, and SWIR. The model also fitted well many of the spectral reflectance features such as reflectance peaks, troughs and valleys, and slopes. Sand layer samples of thickness up to 1.58 g/cm^2 (corresponding to a sand layer thickness of ca. 9.7 mm) were used in this study and was found to be sufficient at wavelengths such as 550 nm, 800 nm, and 1200 nm, but not for 1800 nm. Hence, we expect the model fit to potentially be further improved if measurements at sufficiently thick sand layers is conducted over the whole wavelength range in future studies.

Figure 5 also highlights a weakness in the model that limits its general applicability. We see that all the curves in Figure 5 (both the sand layers on top of the textile, the bare textile and the pure sand with no textile underneath it) obtain near-identical reflectance values at ca. 780 nm. As we will see later in this paper (section 4.3) the estimation of the material parameter, the extinction coefficient, becomes more uncertain as the data points of all the layers and textile become too identical. In such cases, even small measurement errors will affect the model estimation accuracy to a higher degree. A possible solution to this apparent model limitation would be to vary the signature of the underlying textile (white, black, colored) between sand layer measurement series.

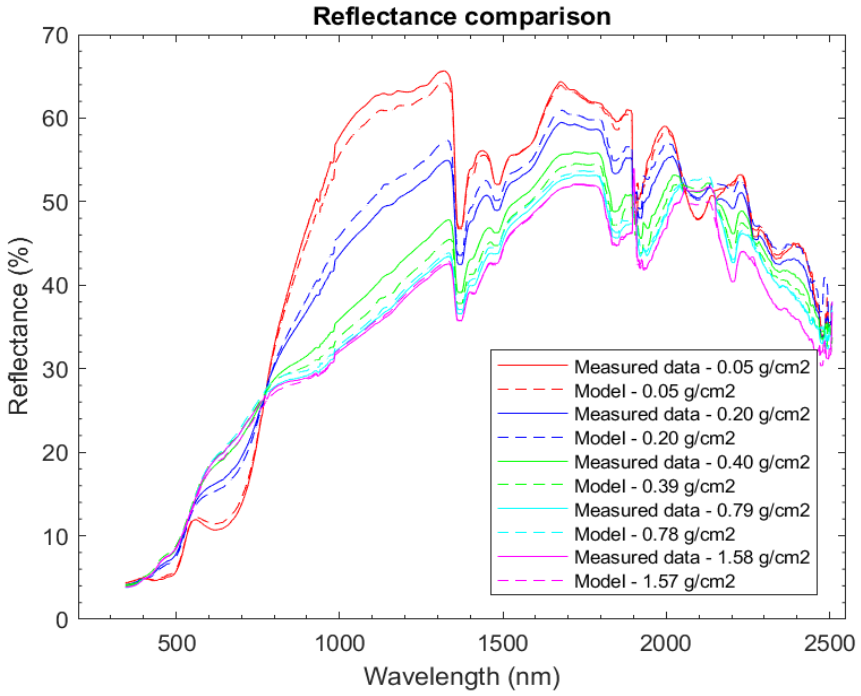

Figure 5. Comparing model reflectance estimations with the experimental reflectance measurements in the wavelength region 345 - 2500 nm. The solid lines show the measured reflectance for the five different sand layer thicknesses and the dotted lines show the corresponding estimated reflectance values from the model.

4.3 Model estimations of the extinction coefficients and reflectance of sand

In Figure 6 we present the model estimations of the extinction coefficient, *k*, (red dots) and the reflectivity, α, (blue dots) of sand based on the experimental reflectance data. Applying the extinction model to the experimental data, makes it possible to estimate the two inherent sand material parameters (*k* and α) for all wavelengths between 345 nm and 2500 nm. Generally, the higher the extinction coefficient, the thinner a sand layer (covering an object) needs to be until no light reaches the underlying object, and the reflectance measured is solely given by the sand optical properties, and the corresponding reflectance value is converging towards the reflectivity of sand (reflectivity of sand is the reflectance of an infinitely thick sand layer).

Regarding the estimations of the extinction coefficient, k, Figure 6 shows that it is largest in the visible wavelength region (ca. 400-750 nm), and that it varies a lot even within that region. For wavelengths longer than 900 nm, the extinction coefficient curve has a decreasing trend towards higher wavelengths, which means that the model estimates the sand layers to be less transparent in the visual range than in NIR and SWIR and also that the sand layers are expected to be more transparent (to incident sunlight) as the wavelength increases. This corresponds with what we found in the reflectance measurements (Fig. 3) where the reflectance of the sand layers (on top of the reference textile) converged more rapidly towards a stable reflectance value (i.e. towards the reflectivity of sand, the inherent optical material parameter) as a function of sand layer thickness for the wavelengths in the visible range compared to longer wavelengths.

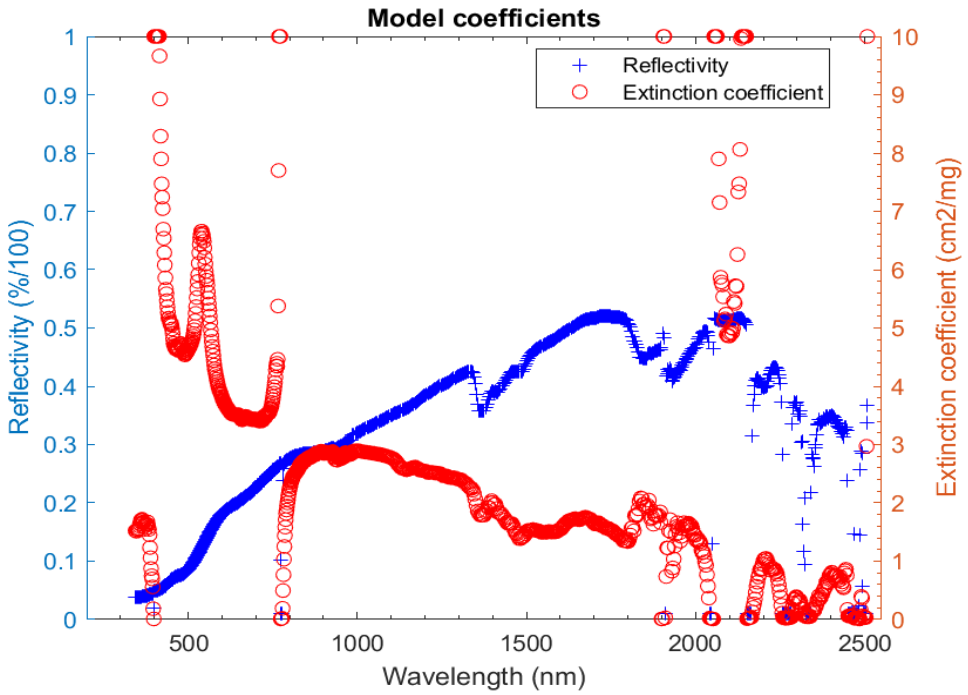

Figure 6. Model estimations of the sand reflectivity (reflectance of an infinitely thick sand layer, blue curve) and the corresponding extinction coefficient over the entire wavelength range. The estimated parameters are based on fitting the extinction model to the experimental reflectance data.

In the visible wavelength region, we see that the estimated k-values (Fig. 6, red curve) greatly varied, being at the largest at 400 nm, then decreasing until ca. 500 nm, followed by an increase to a local maximum at ca. 550 nm, and then further decreasing at longer wavelengths. The experimental reflectance data in Figure 3 can explain to the estimated k-values in the visible range: In Figure 3, the measured reflectance varied less with increasing sand layer thickness at 400 nm (large estimations of *k* in Fig. 6) than at 500 nm (smaller estimations of *k* in Fig. 6). Moreover, the reflectance varied less with sand layer thickness at 550 nm (local peak estimation of *k* in Fig. 6) than with sand layer thickness from 550 nm towards (reduced estimations of *k* in Fig. 6). This correlates with the interpretation that the higher the extinction coefficient of sand, the more rapidly a sand covered target will be masked when the sand layer thickness is gradually increased.

In Figure 6 we also note that there are some wavelength regions in which the estimations of the extinction coefficient (red circles) seem to be undefined or un-reliable. For example at ca. 390-400 nm and at ca. 770-780 nm, the curve of the estimated extinction coefficient is non-continuous, showing vertically asymptotic behavior. A possible explanation to the apparent un-physical behavior of the extinction coefficient at these two wavelength regions can be found in Figure 3. If we inspect the same regions in Figure 3 (390-400 nm and 770-780 nm) we see that all the reflectance curves show a complete or near-complete overlap in the two regions. This means that the reflectance of the reference target and the reflectivity of sand (e.g. the reflectance of pure sand) were identical. Hence, as the reference target and the material used to cover it obtain the same reflectance in these regions, it makes no sense to try to estimate the amount of incident light that is being extinct by the sand layers as any new layer on top will give the same (more or less) reflectance value. The model seems limited to the underlying reference target having a sufficiently different reflectivity than the material to be investigated (i.e. the thin layer material). Whenever the signature of the underlying object differs little from the layer materiel, the effect of measurement errors on the model accuracy is also expected to increase. A possible solution to this issue, would be to perform several series of reflectance measurements where the underlying reference material is altered from one series to the next, and, obviously, that the reference materials to be used have a unique and sufficiently different reflectance signature.

In the wavelength region between ca. 2050 nm and 2150 nm, we observe another region in which the estimated extinction coefficient values seem uncertain. Again, if we go back to the experimental reflectance data (Fig. 3) we see that in this wavelength region the reflectance curves of the sand layers (1 L, 4 L, 8 L, 16 L, and 32 L) no longer obtained reflectance

values that were bounded by the corresponding reflectance values of the reference textile and the pure sand sample. In other words this means that all the measured reflectance values of the sand layers were higher (Fig. 3) than both the reference textile and the pure sand sample, which is contra-intuitive, and may be a potential cause that the model estimations are noisy and unreliable for wavelengths between ca. 2050 nm and 2150 nm.

Regarding the estimated reflectivity values, α, shown in Figure 6 (blue), we see that the reflectivity curve increases as a function of wavelength. As the reflectivity of sand is defined as the reflectance when the sand layer thickness approaches infinite, it is interesting to compare the estimated reflectivity values (Fig. 6, blue) with the experimental reflectance data of pure sand (infinitely thick layer) in Figure 3 (red curve). The measured reflectance of the pure sand layer in Figure 3 should therefore be equal to the reflectivity of sand. The estimated sand reflectivity and experimentally measured sand reflectivity show a great deal similarity, which is further illustrated in Figure 7.

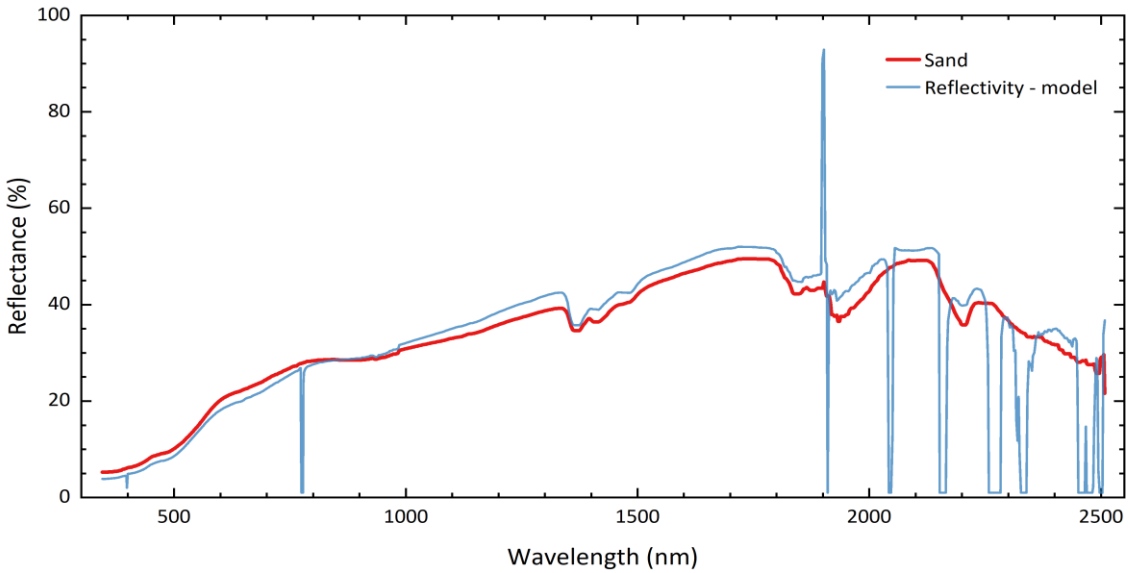

Figure 7. Reflectivity estimated by the extinction model (blue) compared with the experimentally measured reflectivity of sand (red).

4.4 Model estimations of transmittance and absorptance of multiple layered sand layer samples

In Figure 8 we present model estimations of reflectance (R), transmittance (T) and absorptance (A) of one of the sand layers in this study (second thinnest layer; 4 L sand onto reference textile yielding 0.2 g/cm^2). Note that the modelled values of R-T-A are for the 0.2 g/cm^2 sand layer solely, and does not take into account the reflectance properties of the reference textile. Therefore, we see that the reflectance estimations (Fig. 8, red) obtained lower values for all wavelengths relative to the measured reflectance of the same sand layer thickness (Fig. 3, orange), as in the reflectance measurements, the underlying reference textile also contributed to the reflectance. The estimated transmittance (Fig. 8, blue) shows a higher transmittance for wavelengths higher than 900 nm relative to the shorter wavelengths in the visible range. This is as we would expect from the experimental results in Figure 3 where the reflectance converged more rapidly to a fixed reflectance value (the reflectivity) at 500 nm and 650 nm than at 1000 nm and 1800 nm as a function of increasing sand layer thickness. Although not shown explicitly in Figure 8, the amount of incident light that eventually comes back to any external sensor (after having being transmitted through the sand layer, then reflected from the underlying textile and transmitted back through the sand layer) will be given by a two-way transmittance function and modulated by the reflectivity of the underlying target [10, 11].

Note that the extinction coefficients from fitting the reflectance data of the samples (Fig. 4) with the extinction model were in agreement with the absorptance values of the samples (Fig. 8). The extinction coefficient was high at wavelengths where the samples absorbed a high percentage of the light (per mass density unit), and low at wavelengths with low absorptance. For example, at 500 nm, the estimated extinction coefficient was higher than at 1000 nm, and 1800 nm (4.6 > 2.9 > 1.3,

Table 1), and this corresponds with the corresponding values of the estimated absorptance at 500 nm, 1000 nm, and 1800 nm (green curve, Fig. 8).

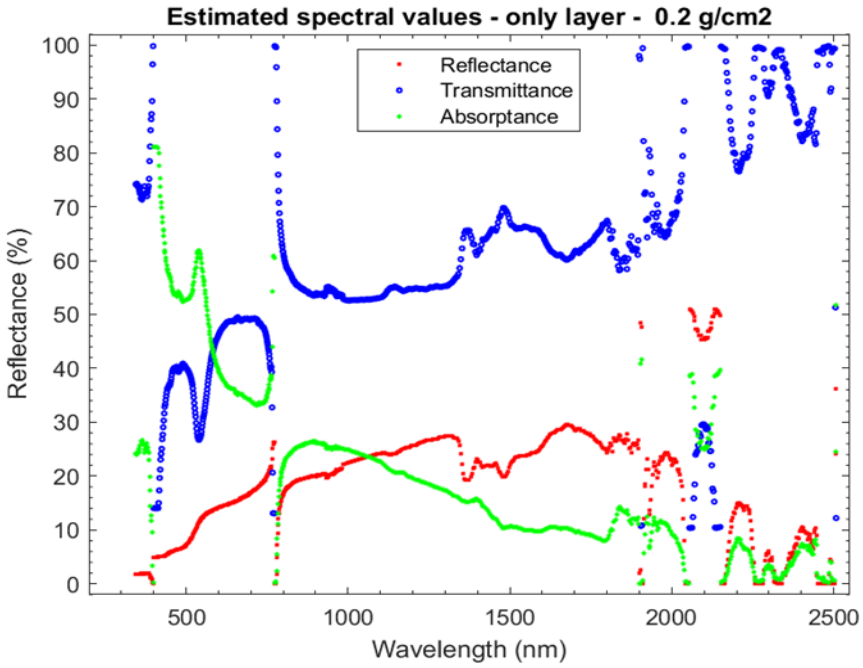

Figure 8. Model estimated reflectance (red), transmittance (blue) and absorptance (green) of a sand layer thickness of 0.2 g/cm^2, which corresponds to 4 L of sand distributed over the reference textile area. The modelled reflectance, transmittance, and absoptance are for the sand layer solely, and does not contain contributions from the underlying reference textile reflectance.

5 CONCLUSIONS AND FUTURE WORK

In this work, we have measured the reflectance of sand layers, of varying thicknesses, on top of a reference textile in the wavelength region from 345 nm to 2500 nm. The reflectance measurements of sand layer samples of varying thicknesses, made it possible to study how sand layers, covering an underlying target, will affect the spectral reflectance properties of the target when being measured through the sand coverage.

At selected wavelengths between 500-2200 nm, the measured reflectance of the sand layer samples were fitted to a mathematical model, known from previous studies as the extinction model [10-12, 15]. The model treats the sample layers as stacked (thin) plates with wavelength-dependent reflectivity and energy loss. The extinction model fitted the measured reflectance data well at the selected wavelengths. Using the fitting parameters (reflectivity and extinction coefficient, Table 1 and Fig. 6) we could also estimate the transmittance and absorptance of light in the sand layer material. We found that the sand layers we measured were less transparent, given by the extinction coefficient, k, to incident light in the visible range (500 nm, $k = 4.6\ cm^2/g$), than in the NIR-range (1000 nm, $k = 2.9\ cm^2/g$), and in the SWIR-range (1800 nm, $k = 1.3\ cm^2/g$), meaning that a sand layer of less than 2 mm yielded a substantial masking of the underlying reference textile signature in the visible range, whereas in the SWIR range a corresponding sand layer thickness of more than 1 cm would be needed.

It is interesting to see that the extinction model seems applicable to describe light penetration into layers of sand material. The model has earlier been shown to be valuable in modelling penetration of incident light into very different materials such as biomaterials (oak [10] and birch [11] leaves), synthetic materials [9, 10], and snow [12]. Hence, the model fit shown in this study therefore seem to support results from other studies, in which it has been reported on similarities in optical properties of granular materials, such as soil and snow, when studying them on length scales much larger than the wavelength [13]. It is also interesting to be able to compare the rough estimates of thicknesses needed of some layer

material in order to mask an underlying reference textile reflectance signature to some given degree. For wet snow it has been showed [12] that thicknesses between 5-10 cm are needed in the visible range, for leaves such as oak [10] or birch [11] 2-3 layers is sufficient in the visible range, and as we have seen in this study a sand layer of 2-3 mm thickness will be effective in the visible range. At higher wavelengths, such as 1800 nm, the corresponding thicknesses are approximately 2 cm (snow), 3-4 layers (oak leaves) and 1 cm (sand).

Overall, the results of this study show that the extinction model has great potential for estimating reflectance of sand layers also at layer thicknesses that have not been measured. The estimations of the extinction coefficients seemed promising and may be valuable in cases where it is of interest to estimate how thick a sand layer needs to be before the reflectance signature of an underlying object is reduced by some given (and wavelength-dependent) factor. It is also worth underlining that the results in this study are preliminary and assigned with some uncertainty, particularly regarding sand layer uniformity and thickness variations in the experiments (particularly the thinnest sand layer), the low number of sand layered studied, number of measurements performed at each sand layer, sand density estimations, and sand volumes used per layer. Still, the overall impression from our experiments is that the extinction model seems promising in modelling light penetration through natural materials such as sand, and that it has potential applications within other fields such as agriculture [10, 11, 14, 43, 55-62], remote sensing applications [13, 46-48, 50, 53, 57, 63], planetary science [41, 44, 45] or solar energy harvesting [35-45] and that further studies are likely to improve the model fit and material optical parameters (reflectivity and extinction coefficient) further.

Future studies should investigate more on how well suited the model is when applied to transmittance and absorptance data of sand (or other soil materials). It would also be of interest to apply the model to data from different sand types and sand with varying moisture content. In addition, the experiments presented in this study should be followed up with more data for each layer thickness, increased number of individual layers, and finally by varying the signature of the underlying reference material.

ACKNOWLEDGMENTS

The works was funded by The Norwegian Defence and Research Establishment (FFI).

The authors have no conflicts of interests.

REFERENCES

[1] G. Selj and M. Søderblom, *Discriminating between camouflaged targets by their time of detection by a human-based observer assessment method* (SPIE Security + Defence). SPIE, 2015.

[2] I. C. Cuthill, M. Stevens, J. Sheppard, T. Maddocks, C. A. Párraga, and T. S. Troscianko, "Disruptive coloration and background pattern matching," *Nature*, vol. 434, no. 7029, pp. 72-74, 2005/03/01 2005.

[3] M. Friškovec and H. Gabrijelčič, "Development of a procedure for camouflage pattern design," *Fibres & Textiles in Eastern Europe*, vol. 18, no. 4, p. 81, 2010.

[4] M. A. Hogervorst, A. Toet, and P. Jacobs, "Design and evaluation of (urban) camouflage," *SPIE Defense, Security, and Sensing*, vol. 7662, 2010.

[5] J. Jersblad and C. Larsson, "Camouflage effectiveness of static nets in SAR images," in *Proc. SPIE*, 2015, vol. 9653: Proc. SPIE, in Proc. SPIE, 2015. [Online]. Available: https://doi.org/10.1117/12.2194321. [Online]. Available: https://doi.org/10.1117/12.2194321

[6] H. Kariis and C. Åkerlind, *Overview of the adaptive camouflage for the soldier II (ACAMSII)* (SPIE Security + Defence). SPIE, 2021.

[7] J. Loyd and J. Sanders, *Physically realistic camouflage net models for visualization and signature generation* (Aerospace/Defense Sensing, Simulation, and Controls). SPIE, 2001.

[8] S. Merilaita, N. E. Scott-Samuel, and I. C. Cuthill, "How camouflage works," *Philosophical Transactions of the Royal Society B: Biological Sciences*, vol. 372, no. 1724, p. 20160341, 2017.

[9] A. Mikkelsen and G. Selj, *Spectral reflectance and transmission properties of a multi-layered camouflage net: comparison with natural birch leaves and mathematical models* (SPIE Security + Defence). SPIE, 2020.

[10] A. Mikkelsen and G. Selj, *Spectral properties of multilayered oak leaves and a camouflage net: experimental measurements and mathematical modelling* (SPIE Security + Defence). SPIE, 2021.
[11] A. Mikkelsen and G. Selj, "Spectral characteristics of moist birch leaves and synthetic materials: experimental studies and evaluation of models," *Optical Engineering*, vol. 60, no. 11, p. 117102, 2021. [Online]. Available: https://doi.org/10.1117/1.OE.60.11.117102.
[12] G. Selj and A. Mikkelsen, *Spectral reflectance measurements of snow and snow covered objects: experimental studies compared with mathematical models* (SPIE Security + Defence). SPIE, 2021.
[13] D. Bänninger and H. Flühler, "Modeling light scattering at soil surfaces," *IEEE TRANSACTIONS ON GEOSCIENCE AND REMOTE SENSING*, vol. 42, no. 7, 2004.
[14] O. Lillesaeter, "Spectral reflectance of partly transmitting leaves: Laboratory measurements and mathematical modeling," *Remote Sensing of Environment*, vol. 12, no. 3, pp. 247-254, 1982/07/01/ 1982, doi: https://doi.org/10.1016/0034-4257(82)90057-8.
[15] R. H. Wilhelm and J. B. Smith, "Transmittance, Reflectance, and Absorptance of Near Infrared Radiation in Textile Materials," *Textile Research Journal*, vol. 19, no. 2, pp. 73-88, 1949, doi: 10.1177/004051754901900202.
[16] Y. Lv, J. Zhang, Y. Dai, A. Li, N. Barnes, and D. P. Fan, "Toward Deeper Understanding of Camouflaged Object Detection," *IEEE Transactions on Circuits and Systems for Video Technology*, vol. 33, no. 7, pp. 3462-3476, 2023, doi: 10.1109/TCSVT.2023.3234578.
[17] G. Selj, "Disruptive camouflage tricks the human eye: a study of detection times of two near-similar targets in natural backgrounds," in *Proc. SPIE*, 2015, vol. 9653: Proc. SPIE, in Proc. SPIE, 2015. [Online]. Available: https://doi.org/10.1117/12.2194157. [Online]. Available: https://doi.org/10.1117/12.2194157
[18] G. Selj and D. Heinrich, "A field-based method for evaluating thermal properties of static and mobile camouflage," in *Proc. SPIE*, 2018, vol. 10794: SPIE, in Proc. SPIE, 2018. [Online]. Available: https://doi.org/10.1117/12.2326981. [Online]. Available: https://doi.org/10.1117/12.2326981
[19] K. B. Toh and P. Todd, "Camouflage that is spot on! Optimization of spot size in prey-background matching," *Evolutionary Ecology*, journal article vol. 31, no. 4, pp. 447-461, August 01 2017.
[20] X. Yin, Q. Chen, and N. Pan, "A study and a design criterion for multilayer-structure in perspiration based infrared camouflage," *Experimental Thermal and Fluid Science*, vol. 46, pp. 211-220, 2013/04/01/ 2013, doi: https://doi.org/10.1016/j.expthermflusci.2012.12.013.
[21] A. Toet and M. Hoogervorst, "Review of camouflage assessment techniques," in *Signature Management Systems Concepts and Integration (SCI) Panel SCI-319 Symposium on 'Signature Management'Brno, Czech Republic, 7-8 May 2019, 1-36*, 2019, in Signature Management Systems Concepts and Integration (SCI) Panel SCI-319 Symposium on 'Signature Management'Brno, Czech Republic, 7-8 May 2019, 1-36, 2019.
[22] D. Heinrich and G. K. Selj, "Evaluation of camouflage pattern performance of textiles by human observers and CAMAELEON," *Proc. SPIE*, vol. 10432, p. 1043206, 2017.
[23] C. M. Birkemark, "CAMEVA: a methodology for computerized evaluation of camouflage effectiveness and estimation of target detectability," *AeroSense '99*, vol. 3699, 1999.
[24] C.-C. Chang, Y.-H. Lee, C. J. Lin, B.-S. Liu, and Y.-C. Shih, "Visual Assessment of Camouflaged Targets with Different Background Similarities," *Perceptual and Motor Skills*, vol. 114, no. 2, pp. 527-541, 2012, doi: 10.2466/24.Pms.114.2.527-541.
[25] J. Culpepper, R. Messina, and V. Wheaton, *Comparison of maritime target detection in field observation, photosimulation and videosimulation* (SPIE Security + Defence). SPIE, 2020.
[26] F. M. Gretzmacher, G. S. Ruppert, and S. Nyberg, "Camouflage assessment considering human perception data," *Aerospace/Defense Sensing and Controls*, vol. 3375, 1998.
[27] A. Hossain, "Spectral simulation and method design of camouflage textiles for concealment of hyperspectral imaging in UV-Vis-IR against multidimensional combat background," *The Journal of The Textile Institute*, vol. 114, no. 2, pp. 331-342, 2023/02/01 2023, doi: 10.1080/00405000.2022.2027074.
[28] N. Li, L. Li, J. Jiao, W. Xu, W. Qi, and X. Yan, "Research status and development trend of image camouflage effect evaluation," *Multimedia Tools and Applications*, vol. 81, no. 21, pp. 29939-29953, 2022/09/01 2022, doi: 10.1007/s11042-022-12287-3.
[29] R. Messina and J. Culpepper, *Field observation, photosimulation and videosimulation of target detection in maritime environments: update* (SPIE Security + Defence). SPIE, 2021.
[30] F. Racek, T. Baláž, and J. Krejčí, *Evaluation of target acquisition performance in photosimulation test* (SPIE Security + Defence). SPIE, 2019.

[31] G. Ruppert, R. Beichel, and F. Gretzmacher, *Robust measure for camouflage effectiveness in the visual domain* (AeroSense 2000). SPIE, 2000.
[32] A. Schwegmann, "Camouflage evaluation by bio-inspired local conspicuity quantification," *Proc. SPIE*, vol. 10794, p. 107940H, 2018.
[33] D. Heinrich and G. Selj, "The effect of contrast in camouflage patterns on detectability by human observers and CAMAELEON," in *Proc. SPIE*, 2015, vol. 9476: SPIE, in Proc. SPIE, 2015. [Online]. Available: https://doi.org/10.1117/12.2176968. [Online]. Available: https://doi.org/10.1117/12.2176968
[34] A. Toet and M. Hogervorst, "Urban camouflage assessment through visual search and computational saliency," *Optical Engineering*, vol. 52, no. 4, p. 041103, 2012.
[35] T. Salamah *et al.*, "Effect of dust and methods of cleaning on the performance of solar PV module for different climate regions: Comprehensive review," *Science of The Total Environment*, vol. 827, p. 154050, 2022.
[36] M. R. Maghami, H. Hizam, C. Gomes, M. A. Radzi, M. I. Rezadad, and S. Hajighorbani, "Power loss due to soiling on solar panel: A review," *Renewable and Sustainable Energy Reviews*, vol. 59, pp. 1307-1316, 2016.
[37] T. Sarver, A. Al-Qaraghuli, and L. L. Kazmerski, "A comprehensive review of the impact of dust on the use of solar energy: History, investigations, results, literature, and mitigation approaches," *Renewable and sustainable energy Reviews*, vol. 22, pp. 698-733, 2013.
[38] M. Rahman, M. Hasanuzzaman, and N. A. Rahim, "Effects of various parameters on PV-module power and efficiency," *Energy Conversion and Management*, vol. 103, pp. 348-358, 2015.
[39] H. Jiang, L. Lu, and K. Sun, "Experimental investigation of the impact of airborne dust deposition on the performance of solar photovoltaic (PV) modules," *Atmospheric environment*, vol. 45, no. 25, pp. 4299-4304, 2011.
[40] K. C. Lakshmi and G. Ramadas, "Dust Deposition's effect on solar photovoltaic module performance: An experimental study in India's tropical region," *J. Renew. Mater*, vol. 10, pp. 2133-2153, 2022.
[41] P. Jenkins *et al.*, "A dust characterization experiment for solar cells operating on Mars," in *Conference Record of the Twenty-Eighth IEEE Photovoltaic Specialists Conference-2000 (Cat. No. 00CH37036)*, 2000: IEEE, pp. 1358-1361.
[42] T. Kjeldstad *et al.*, "The performance and amphibious operation potential of a new floating photovoltaic technology," *Solar Energy*, vol. 239, pp. 242-251, 2022.
[43] H. Pedersen, J. Strauss, and J. Selj, "Effect of soiling on photovoltaic modules in Norway," *Energy Procedia*, vol. 92, pp. 585-589, 2016.
[44] G. A. Landis, P. Jenkins, J. Flatico, L. Oberle, M. Krasowski, and S. Stevenson, "Development of a Mars dust characterization instrument," *Planetary and Space Science*, vol. 44, no. 11, pp. 1425-1433, 1996.
[45] G. Mongelluzzo *et al.*, "CFD analysis and optimization of the sensor "MicroMED" for the ExoMars 2020 mission," *Measurement*, vol. 147, p. 106824, 2019.
[46] Y. Y. Aldakheel and F. M. Danson, "Spectral reflectance of dehydrating leaves: Measurements and modelling," *International Journal of Remote Sensing*, vol. 18, no. 17, pp. 3683-3690, 1997/11/01 1997, doi: 10.1080/014311697216883.
[47] L. Liu, J. Wang, W. Huang, and C. Zhao, "Detection of leaf and canopy EWT by calculating REWT from reflectance spectra," *International Journal of Remote Sensing*, vol. 31, no. 10, pp. 2681-2695, 2010/05/20 2010, doi: 10.1080/01431160903085636.
[48] D. A. Sims and J. A. Gamon, "Relationships between leaf pigment content and spectral reflectance across a wide range of species, leaf structures and developmental stages," *Remote Sensing of Environment*, vol. 81, no. 2, pp. 337-354, 2002/08/01/ 2002, doi: https://doi.org/10.1016/S0034-4257(02)00010-X.
[49] L. Wang, J. J. Qu, X. Hao, and E. R. Hunt, "Estimating dry matter content from spectral reflectance for green leaves of different species," *International Journal of Remote Sensing*, vol. 32, no. 22, pp. 7097-7109, 2011/11/20 2011, doi: 10.1080/01431161.2010.494641.
[50] Z. Zhu, "Change detection using landsat time series: A review of frequencies, preprocessing, algorithms, and applications," *ISPRS Journal of Photogrammetry and Remote Sensing*, vol. 130, pp. 370-384, 2017.
[51] J. Padarian, B. Minasny, and A. McBratney, "Using deep learning to predict soil properties from regional spectral data," *Geoderma Regional*, vol. 16, p. e00198, 2019.
[52] M. Nocita, A. Stevens, G. Toth, P. Panagos, B. van Wesemael, and L. Montanarella, "Prediction of soil organic carbon content by diffuse reflectance spectroscopy using a local partial least square regression approach," *Soil Biology and Biochemistry*, vol. 68, pp. 337-347, 2014.

[53] A. Gholizadeh, D. Žižala, M. Saberioon, and L. Borůvka, "Soil organic carbon and texture retrieving and mapping using proximal, airborne and Sentinel-2 spectral imaging," *Remote Sensing of Environment*, vol. 218, pp. 89-103, 2018.

[54] G. G. Stokes, "IV. On the intensity of the light reflected from or transmitted through a pile of plates," *Proceedings of the Royal Society of London*, vol. 11, pp. 545-556, 1862, doi: doi:10.1098/rspl.1860.0119.

[55] P. Bowyer and F. M. Danson, "Sensitivity of spectral reflectance to variation in live fuel moisture content at leaf and canopy level," *Remote Sensing of Environment*, vol. 92, no. 3, pp. 297-308, 2004/08/30/ 2004, doi: https://doi.org/10.1016/j.rse.2004.05.020.

[56] P. Ceccato, S. Flasse, S. Tarantola, S. Jacquemoud, and J.-M. Grégoire, "Detecting vegetation leaf water content using reflectance in the optical domain," *Remote Sensing of Environment*, vol. 77, no. 1, pp. 22-33, 2001/07/01/ 2001, doi: https://doi.org/10.1016/S0034-4257(01)00191-2.

[57] F. M. Danson and P. Bowyer, "Estimating live fuel moisture content from remotely sensed reflectance," *Remote Sensing of Environment*, vol. 92, no. 3, pp. 309-321, 2004/08/30/ 2004, doi: https://doi.org/10.1016/j.rse.2004.03.017.

[58] J. B. Féret *et al.*, "Estimating leaf mass per area and equivalent water thickness based on leaf optical properties: Potential and limitations of physical modeling and machine learning," *Remote Sensing of Environment*, vol. 231, p. 110959, 2019/09/15/ 2019, doi: https://doi.org/10.1016/j.rse.2018.11.002.

[59] A. Gitelson and M. N. Merzlyak, "Spectral Reflectance Changes Associated with Autumn Senescence of Aesculus hippocastanum L. and Acer platanoides L. Leaves. Spectral Features and Relation to Chlorophyll Estimation," *Journal of Plant Physiology*, vol. 143, no. 3, pp. 286-292, 1994/03/01/ 1994, doi: https://doi.org/10.1016/S0176-1617(11)81633-0.

[60] S. Jacquemoud *et al.*, "PROSPECT+SAIL models: A review of use for vegetation characterization," *Remote Sensing of Environment*, vol. 113, pp. S56-S66, 2009/09/01/ 2009, doi: https://doi.org/10.1016/j.rse.2008.01.026.

[61] W. RIPPLE, "Spectral reflectance relationships to leaf water stress," *Photogrammetric Engineering and Remote Sensing*, vol. 52, no. 10, pp. 1669-1675, 1986.

[62] D. A. Sims and J. A. Gamon, "Estimation of vegetation water content and photosynthetic tissue area from spectral reflectance: a comparison of indices based on liquid water and chlorophyll absorption features," *Remote Sensing of Environment*, vol. 84, no. 4, pp. 526-537, 2003/04/10/ 2003, doi: https://doi.org/10.1016/S0034-4257(02)00151-7.

[63] L. Liu, S. Zhang, and B. Zhang, "Evaluation of hyperspectral indices for retrieval of canopy equivalent water thickness and gravimetric water content," *International Journal of Remote Sensing*, vol. 37, no. 14, pp. 3384-3399, 2016/07/17 2016, doi: 10.1080/01431161.2016.1199083.